

Increased preferential activation of small cutaneous nerve fibers by optimization of electrode design parameters

Poulsen, Aida Hejlskov; Tigerholm, Jenny; Andersen, Ole Kaeseler; Mørch, Carsten Dahl

Published in:
Journal of Neural Engineering

DOI (link to publication from Publisher):
[10.1088/1741-2552/abd1c1](https://doi.org/10.1088/1741-2552/abd1c1)

Creative Commons License
CC BY-NC-ND 3.0

Publication date:
2021

Document Version
Accepted author manuscript, peer reviewed version

[Link to publication from Aalborg University](#)

Citation for published version (APA):
Poulsen, A. H., Tigerholm, J., Andersen, O. K., & Mørch, C. D. (2021). Increased preferential activation of small cutaneous nerve fibers by optimization of electrode design parameters. *Journal of Neural Engineering*, 18(1), Article 016020. <https://doi.org/10.1088/1741-2552/abd1c1>

General rights

Copyright and moral rights for the publications made accessible in the public portal are retained by the authors and/or other copyright owners and it is a condition of accessing publications that users recognise and abide by the legal requirements associated with these rights.

- Users may download and print one copy of any publication from the public portal for the purpose of private study or research.
- You may not further distribute the material or use it for any profit-making activity or commercial gain
- You may freely distribute the URL identifying the publication in the public portal -

Take down policy

If you believe that this document breaches copyright please contact us at vbn@aub.aau.dk providing details, and we will remove access to the work immediately and investigate your claim.

ACCEPTED MANUSCRIPT

Increased preferential activation of small cutaneous nerve fibers by optimization of electrode design parameters

To cite this article before publication: Aida Hejlskov Poulsen *et al* 2020 *J. Neural Eng.* in press <https://doi.org/10.1088/1741-2552/abd1c1>

Manuscript version: Accepted Manuscript

Accepted Manuscript is “the version of the article accepted for publication including all changes made as a result of the peer review process, and which may also include the addition to the article by IOP Publishing of a header, an article ID, a cover sheet and/or an ‘Accepted Manuscript’ watermark, but excluding any other editing, typesetting or other changes made by IOP Publishing and/or its licensors”

This Accepted Manuscript is © 2020 IOP Publishing Ltd.

During the embargo period (the 12 month period from the publication of the Version of Record of this article), the Accepted Manuscript is fully protected by copyright and cannot be reused or reposted elsewhere.

As the Version of Record of this article is going to be / has been published on a subscription basis, this Accepted Manuscript is available for reuse under a CC BY-NC-ND 3.0 licence after the 12 month embargo period.

After the embargo period, everyone is permitted to use copy and redistribute this article for non-commercial purposes only, provided that they adhere to all the terms of the licence <https://creativecommons.org/licenses/by-nc-nd/3.0>

Although reasonable endeavours have been taken to obtain all necessary permissions from third parties to include their copyrighted content within this article, their full citation and copyright line may not be present in this Accepted Manuscript version. Before using any content from this article, please refer to the Version of Record on IOPscience once published for full citation and copyright details, as permissions will likely be required. All third party content is fully copyright protected, unless specifically stated otherwise in the figure caption in the Version of Record.

View the [article online](#) for updates and enhancements.

1
2
3
4
5
6
7
8
9
10
11
12
13
14
15
16
17
18
19
20
21
22
23
24
25
26
27
28
29
30
31
32
33
34
35
36
37
38
39
40
41
42
43
44
45
46
47
48
49
50
51
52
53
54
55
56
57
58
59
60

Increased preferential activation of small cutaneous nerve fibers by optimization of electrode design parameters.

Authors: Aida Hejlskov Poulsen*, Jenny Tigerholm*, Ole Kæseler Andersen*, Carsten Dahl Mørch*

*Center for Neuroplasticity and Pain (CNAP), Department of Health Science and Technology, Aalborg University, Aalborg, Denmark

Abstract

Objective. Electrical preferential activation of small nociceptive fibers may be achieved with the use of specialized small area electrodes, however, the existing electrodes are limited to low stimulation intensities. As existing electrodes have been developed empirically, the present study aimed to use computational modeling and optimization techniques to investigate if changes in electrode design parameters could improve the preferential activation of small fibers.

Approach. Two finite element models; one of a planar concentric and one of an intra-epidermal electrode were combined with two multi-compartmental nerve fiber models of an A δ -fiber and an A β -fiber. These two-step hybrid models were used for the optimization of four electrode parameters; anode area, anode-cathode distance, cathode area, and cathode protrusion. Optimization was performed using a gradient-free bounded Nelder-Mead algorithm, to maximize the current activation threshold ratio between the A β -fiber model and the A δ -fiber model.

Main results. All electrode parameters were optimal at their lower bound, except the cathode protrusion, which was optimal a few micrometers above the location of the A δ -fiber model. A small cathode area is essential for producing a high current density in the epidermal skin layer enabling activation of small fibers, while a small anode area and anode-cathode distance are important for the minimization of the current spread to deeper tissues, making it less likely to activate large fibers. Combining each of the optimized electrode parameters improved the preferential activation of small fibers in comparison to existing electrodes, by increasing the activation threshold ratio between the two nerve fiber types. The maximum increase in the

activation threshold ratio was 289% and 595% for the intra-epidermal and planar concentric design, respectively.

Significance. The present study showed that electrical preferential small fiber activation can be improved by electrode design. Additionally, the results may be used for the production of an electrode that could potentially be used for clinical assessment of small fiber neuropathy.

1. Introduction

Electrical stimulation is often used to probe and evaluate the status of the somatosensory system, as it is a reproducible, easy to control, and safe method. However, conventional electrical stimulation performed with large area patch electrodes lacks specificity of fiber type activation and provides a mixed afferent input to the central nervous system. Consequently, it becomes difficult to interpret and distinguish the contributions from different sensory subsystems such as the touch and pain systems. The electrical activation threshold for large tactile A β -fibers is lower than that of small nociceptive A δ - and C-fibers, which makes it possible to preferentially activate large fibers and thereby primarily activate the touch system, provided that non-painful stimulation intensities are used. Preferential activation of the pain pathways is not feasible by the conventional electrical stimulation setup, as even painful stimulation intensities would co-activate a large proportion of non-nociceptive fibers. To overcome this limitation, specialized concentric, small area, electrodes have been developed [1]–[4]. These electrode designs take advantage of the difference in the termination depth of small and large cutaneous nerve fibers. The small fibers terminate in the epidermal skin layer [5] and the large fibers deeper in the dermis [6]. Accordingly, the specialized electrodes produce a higher electrical field in the epidermis and limit the current spread to deeper skin structures [1], [7], [8]. The suggestion that these electrodes preferentially activate small fibers has been supported by experimental observations of delayed reaction times [9],[10], and cortical responses [11]–[13], in addition to the electrodes eliciting pinprick-like sensations [1]–[4]. Furthermore, computational studies have confirmed the ability of the electrodes to preferentially activate small cutaneous nerve fibers [10] and demonstrated the importance of a small cathode area [7]. A small cathode area produces a higher current density in the proximity of the electrode and thus a higher current density in the more superficial skin layers, enabling the electrode to activate small fibers at a lower intensity than large fibers. Consequently, such electrodes have been suggested as a tool for the assessment of small fiber function in neuropathic

pain patients [14]–[16]. However, co-activation of large non-nociceptive fibers has been observed in healthy subjects [11], [17] and the application of the electrodes are limited to low stimulation intensities, as the amount of co-activation increases with intensity and becomes especially prominent at intensities above approximately two times perception threshold [11], [17], [18]. The co-activation of large fibers would likely be even greater in patients suffering from small fiber neuropathy, as patients have been shown to express decreased intra-epidermal nerve fiber density [19]. Degeneration of the nerve fibers results in a retraction of nerve fiber terminals and would make it more difficult to activate small fibers. The electrode's ability to achieve preferential activation of small fibers would, thereby, be lost in patients with small fiber neuropathy, as higher intensities would be needed to activate the retracting fibers. This indicates the need for an electrode that still produces a high current density in the epidermis but has a more restricted current spread to deeper skin structures, to enable a preferential small fiber activation throughout the epidermal skin layer. Given that existing electrodes have been developed empirically and as only a few studies exist on the influence of different electrode parameters, with particular focus on the cathode design [7], [8], it is believed that the cathode, as well as the anode dimensions of the electrode design, can be further developed to improve the preferential activation of small fibers. Thus, the present study aimed at optimizing electrode design parameters to increase preferential activation of small cutaneous nerve fibers and to investigate the influence that different electrode design parameters have on the distribution of the electrical potential in the skin and the consequent nerve fiber activation.

2. Methods

A planar and an intra-epidermal electrode design were investigated. The models were similar except that the planar electrode did not protrude into the epidermal skin layer, whereas the intra-epidermal design did. A two-step hybrid *in silico* model, developed and validated by Poulsen et al [10], was used to investigate and optimize four electrode design parameters; the anode area, anode-cathode distance, cathode protrusion, and cathode area (see figure 1). The first part of the hybrid model was a finite element model of the electrode and skin [10], from which the electrical potential produced in the skin was calculated and extracted. The electrical potential was subsequently introduced in the second part of the model, containing two multi-compartmental axon models of an A δ - and an A β -fiber axon, describing the nerve fiber activation [20].

The two steps of the model will be briefly described here and the reader is referred to Poulsen et al [10] and Tigerholm et al [20] for detailed descriptions of the skin and nerve fiber models, respectively.

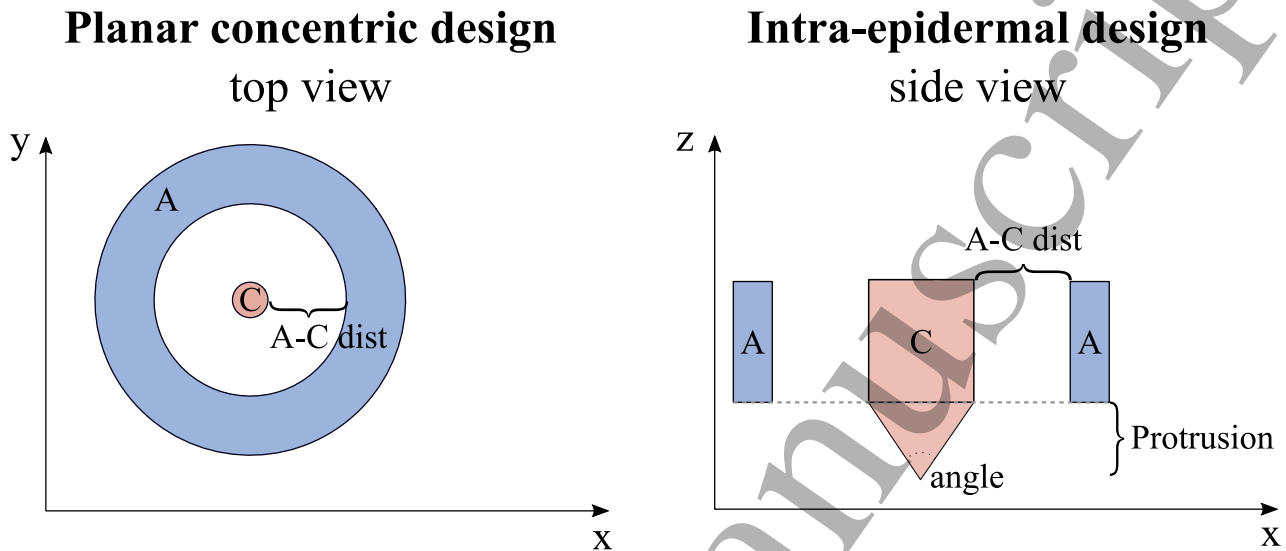


Figure 1: Sketch of a concentric and intra-epidermal electrode design and the investigated electrode design parameters. The anode area (A), the cathode area (C) and the anode-cathode distance (A-C dist) were investigated for both a purely planar design and an intra-epidermal design, for which the cathode penetrated the stratum corneum. The cathode area was investigated for the intra-epidermal design by changing the angle of the needle, and thereby also the diameter. Additionally, the cathode protrusion was investigated for the intra-epidermal design.

2.1 Finite element model of the skin and electrodes

The electrical potentials produced in the skin by electrical stimulations were estimated through finite element models, implemented in COMSOL Multiphysics (5.3, Stockholm, Sweden) as 2D-axisymmetrical models. The models represented a section of the volar forearm and included the electrode-skin interface, the stratum corneum, epidermis, dermis, and hypodermis (see figure 2). All layers were implemented as homogeneous cylindrical skin layers and with a purely horizontal interface between the layers. The electrode-skin interface was implemented as a 10 μm thick layer and was included to accurately model electrode impedance [10]. The electrical conductivity of

the electrode-skin interface was deduced from resistance and capacitance values for dry electrode contacts reported by Chi et al [21]. The epidermis and dermis were considered electrically anisotropic, while the remaining layers were considered isotropic. The electrical properties of the different layers are listed in figure 2.

A quasi-static approximation was used to calculate the extracellular electrical potential, expressed by Laplace formulation:

$$-\nabla \cdot (\sigma \nabla V_{FE} - \mathbf{J}_e) = 0$$

Where σ is the conductivity, V_{FE} is the electrical potential, and \mathbf{J}_e is the external current density, which was applied to the electrode surface by a distributed normal current density condition. An evenly distributed current of 1 mA and -1 mA was applied to the cathode and anode interfaces, respectively. The bottom of the hypodermal skin layer was grounded, and all other external boundaries were considered electrically insulated. Electrical continuity conditions were applied to all inner boundaries. The finite element mesh consisted of free triangular elements. The density of the mesh was highest around the edge of the electrode, where the electrical potential is expected to exhibit a steep decrease. A convergence study of the mesh density and model radius was performed to ensure that these were large enough to get a reliable estimation of the electrical potential. The model radius was increased by 1 cm, and the mesh density was increased by decreasing the maximum and minimum element sizes by 1e-6 m, until the change in electrical potential, at the nerve fiber location, from the previous increment was less than 0.1 mV, which is below the accuracy of the nerve fiber model. The convergence study was conducted for both the minimum and maximum electrode design parameter values used in the optimization (see table 1). Based on the convergence study of the mesh, the maximum and minimum element size for the models were set to 9e-6 m and 0.0016 m, respectively. The maximum growth rate was set to 10% and the average number of elements used were 52,675 for the intra-epidermal electrode design and 46,102 for the planar concentric electrode design. The average *volume versus circumradius* quality of the mesh elements were 0.825 and all elements had a quality above the acceptance limit of 0.1. The final radius of the models was 11 cm.

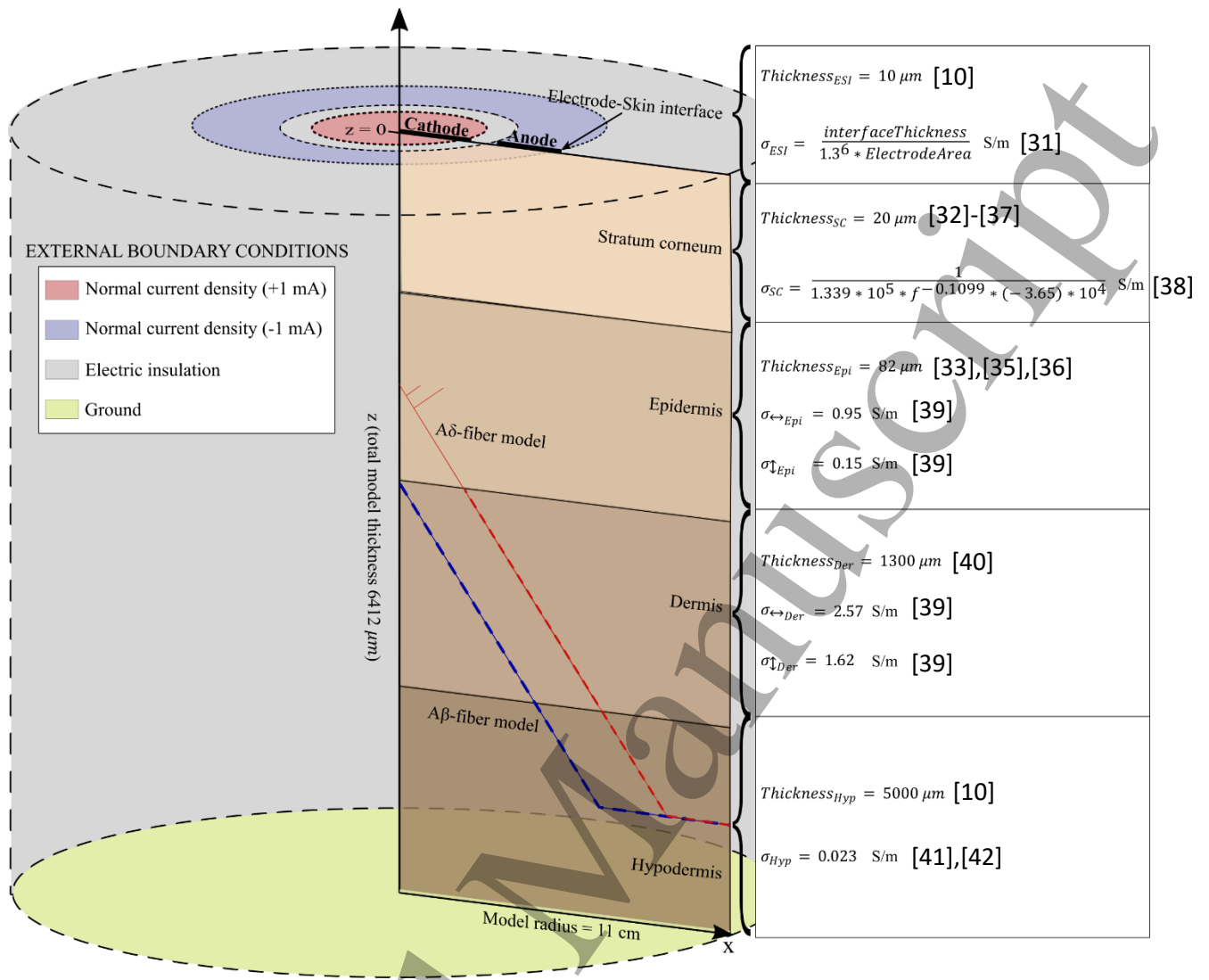


Figure 2: A representation of the 2D axisymmetric model (not drawn in scale). The models consisted of an electrode-skin interface layer and four skin layers; the stratum corneum, epidermis, dermis, and hypodermis, with the specific properties listed to the right [10]. f is the frequency of the applied current in Hz, which in the present study was 1000 Hz, corresponding to a 1 ms stimulation pulse. The electrodes were modeled by the electrode-skin interface on the surface of which an evenly distributed current of 1 mA was applied to the cathode, and a total current of -1 mA was applied to the anode. The bottom of the hypodermal layer was grounded and the radius of the axisymmetric models was 11 cm. The nerve fiber models were located directly under the cathode. The A δ -fiber model ran horizontally in the middle of the hypodermal layer, made a 45-degree bend [20], and branched to the epidermal layer where it branched further, terminating in three free nerve endings in the middle of the epidermis. The A δ -fiber model lost its myelin sheets as it crossed the dermal-epidermal junction [5]. The A β -fiber model ran horizontally in the middle of the hypodermal layer before branching in a 45-degree angle [20] and eventually terminating in the superficial part of the dermis.

1
2
3
4
5
6
7 **2.2 Axon nerve fiber models**

8 The axon models of an A δ -fiber and an A β -fiber were developed by Tigerholm et al [20] and was
9 implemented in the NEURON environment (6.7 NEURON Yale, USA [22]). The A δ -fiber model
10 was 5.472 cm long with 2 compartments per μm (total: 26,088 compartments). The diameter of
11 the A δ -fiber model was 3.5 μm . The A β -fiber model was 4.994 cm long and had 1.8 compartments
12 per μm , corresponding to a total of 27,120 compartments. The diameter of the A β -fiber model was
13 9 μm .

14 Both nerve fiber models ran horizontally in the middle of the hypodermal layer, from where a
15 single branch of 45-degrees [20] ascended through the skin layers before terminating as a free
16 nerve ending in the superficial part of the dermis ($z = -112 \mu\text{m}$) and the middle of the epidermis
17 ($z = -61 \mu\text{m}$), for the A β -fiber model and A δ -fiber model, respectively (see figure 2). The
18 termination points of the models were located directly under the cathode, where the electrical
19 potential was highest. The A β -fiber model location, was quite conservative, considering only a
20 few fibers terminate in the superficial part of the dermis [6]. This position was chosen as a
21 consequence of the nerve fiber termination points in the peak of the electrical potential and to
22 enable investigations of small fiber selectivity. The A δ -fiber model lost its myelination as it
23 crossed the dermal-epidermal junction [5] and branched two additional times (90 degrees) in the
24 epidermis. The A δ -fiber model, thereby, terminated with three nerve fiber endings with an
25 equispaced distance, corresponding to a nerve fiber density of 0.58 nerve fiber endings per
26 millimeter [23]. All implemented ion channels were Hodgkin-Huxley-type ion channels; Nav1.6,
27 Nav1.7, Nav1.8, Nav1.9, K_{dr} , K_{M} , K_{A} , and the hyperpolarization-activated and cyclic nucleotide-
28 gated (HCN) channels.

29 The electrical potential produced by the electrode was extracted from the finite element model, at the
30 nerve fiber location, and added as the extracellular potential to the axon models. A 1 ms monophasic
31 rectangular step function, corresponding to the cathodic stimulation pulse, was multiplied to the
32 extracellular potential and linearly increased to estimate the activation threshold. The activation
33 threshold was defined as the smallest stimulation current sufficient to generate an action potential that
34 propagated to the end of the axon. The model was solved by the variable time step method. For both
35 electrode models, the nerve fiber models were activated at the tip.

36
37
38
39
40
41
42
43
44
45
46
47
48
49
50
51
52
53
54
55
56
57 **2.4 Optimization**

The planar design was optimized for anode area, anode-cathode distance, and cathode area, while the intra-epidermal design was optimized for anode area, anode-cathode distance, cathode area (by changing needle angle), and cathode protrusion. To investigate if the optimal protrusion depends on the nerve fiber termination depth, the optimization of the cathode protrusion was performed for three different nerve fiber termination depths of the A δ -fiber model ($z = -31 \mu\text{m}$, $z = -61 \mu\text{m}$, and $z = -101 \mu\text{m}$, measured from the skin surface, $z=0$). The entire nerve fiber model was moved in the vertical direction, hence leaving the overall nerve fiber morphology intact (see figure 3).

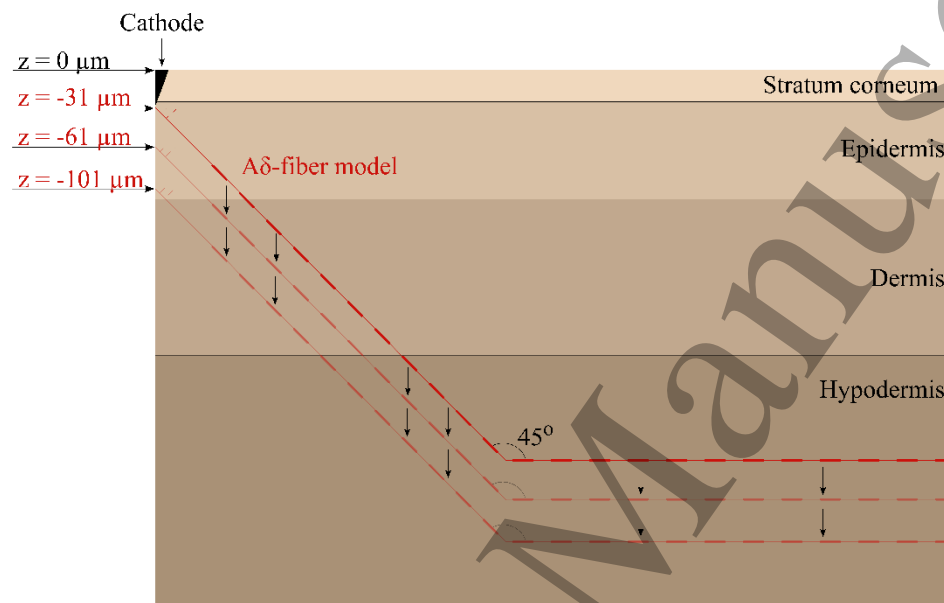


Figure 3: Illustration of how the nerve fiber was moved within the skin (not drawn to scale). The entire nerve fiber was moved, when changing the termination depth of the fiber, keeping the nerve fiber morphology intact.

Optimization was performed a total of three times for each of the individual design parameters while the rest of the parameters were kept constant at the dimensions of the existing planar concentric electrode introduced by Kaube et al [1] and the intra-epidermal electrode introduced by Inui et al [2] (see dimensions in table 1). For the intra-epidermal electrode the penetration depth was, however, changed to $30 \mu\text{m}$, as the electrode is expected to only just penetrate the stratum corneum.

The optimization problem was to maximize the activation threshold ratio between the A β -fiber model and A δ -fiber model. Only the function values were known, and a Globalized Bounded Nelder-Mead (GBNM) algorithm presented by Luersen et al [24] was applied to optimize the

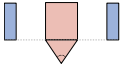

electrode parameters (see supplementary material for a more detailed description of the algorithm). This method is gradient-free and does not depend on derivatives of the objective function, but only on the simulation values (the $A\beta/A\delta$ -fiber model activation ratio) of the hybrid model. The GBMN algorithm introduced restarts to enable the Nelder-Mead algorithm to escape from a collapsed simplex, where the optimization is stuck in a subspace of the search space. Additionally, the restarts minimized the effect that premature termination could have on the results. A second type of restarts, probabilistic restarts using spatial probability [24], where the algorithm was restarted whenever the previous run had converged, was introduced to increase the likelihood of finding the global optimum rather than a local optimum. Convergence was assumed, when one of the three convergence tests; small, flat, or degenerated, were below their respective convergence coefficients (see table 2). The GBMN algorithm terminated when a total of 20 restarts had been performed or the maximum number of function evaluations was reached. Parameter values of the GBMN algorithm are listed in table 2.

The initial step of the GBMN algorithm was to arbitrarily select solutions in the feasible solution space and make up the initial simplex containing $n+1$ vertices, with n denoting the dimensions. The initial simplex consisted of two randomly sampled points between the upper and lower boundary (see supplementary table S1).

. The lower bounds for each of the electrode design parameters were based on fabrication feasibility, and the upper bounds were set to the dimensional values for a regular 1.5x2 cm patch electrode (Ambu® neuroline 700). The bounds are specified in table 1. The original Nelder-Mead algorithm searches for the minimum value [25], however, the negative functional values were used for evaluations in the present study to enable a maximization search (see iterations counts in supplementary table S1).

Table 1: The electrode parameters for which optimization was performed and for which electrode designs (planar or intra-epidermal). The lower and upper bounds that were set as restrictions for the optimization are listed. The bound for the cathode area deviated between the two designs due to restrictions of the possible needle angle. For the needle protrusion optimization was performed for three locations of the $A\delta$ -

fiber model ($z = -31 \mu\text{m}$, $z = -61 \mu\text{m}$, and $z = -101 \mu\text{m}$), and in each case the upper bound for the protrusion was set to $1 \mu\text{m}$ less than the location of the nerve fiber tip.

	Intra-epidermal design 			Planar Concentric design 		
Parameter	Dimensions of original design [2]	Lower bound	Upper bound	Dimensions of original design [1]	Lower bound	Upper bound
Anode area	0.56 mm^2	$6 \times 10^{-4} \text{ m}^2$	3 cm^2	8.64 mm^2	$6 \times 10^{-4} \text{ mm}^2$	3 cm^2
Anode-cathode distance	0.5 mm	$100 \mu\text{m}$	4 cm	2.25 mm	$100 \mu\text{m}$	4 cm
Cathode area	$1.45 \times 10^{-3} \text{ mm}^2$	$6.59 \times 10^{-4} \text{ m}^2$	9.28 m^2	0.20 mm^2	$2.83 \times 10^{-3} \text{ mm}^2$	3 cm^2
Cathode protrusion	$100 \mu\text{m}$ ($30 \mu\text{m}$ used for simulation)	$10 \mu\text{m}$	$30 \mu\text{m}$ $60 \mu\text{m}$ $100 \mu\text{m}$			

	purpo ses)					
--	---------------	--	--	--	--	--

Table 2: Values of the parameters of the GBMN algorithm

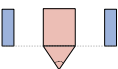

Parameter description	Parameter value
Number of allowed restarts	20
Maximum function evaluations	3000
Reflex coefficient (r)	1
Contraction coefficient (β)	0.5
Expansion coefficient (γ)	2
Small simplex test convergence coefficient (ϵ_{s1})	1e-06
Flat simplex convergence coefficient (ϵ_{s2})	1e-08
Degenerated simplex convergence coefficient (ϵ_{s3} & ϵ_{s4})	1e-06

2.4 Sensitivity analysis

To further evaluate the robustness of the model and its sensitivity to changes in tissue properties, a sensitivity analysis of tissue conductivities was performed for the original electrode dimensions. The investigated ranges of conductivities are listed in table 3, together with the change in the peak electrical potential observed at the locations of the nerve fiber models. The peak potential at the location of the A δ -fiber model changed the most when conductivities of the epidermis were altered. It was clear that an increase in the horizontal conductivity increased the horizontal current spread, which led to a decrease in the potential in the middle of the epidermal layer, where the A δ -fiber model was located. The opposite was true for the vertical direction, where an increase in conductivity also increased the peak potential at the nerve fiber model location. The maximum difference in peak potential when changing the conductivity of the epidermis was observed for the lowest conductivity value. Altering the conductivity of the dermal skin layer resulted in changes for both the peak potential at the A δ -fiber model and the A β -fiber model location. However, the

A β -fiber model location was affected to a larger degree and the changes were largest for alterations of the horizontal conductivity. Changes in stratum corneum conductivity did not affect the intra-epidermal electrode design. This is likely due to the fact that the intra-epidermal electrode penetrates the stratum corneum layer. The planar concentric electrode design was more affected by changes in stratum corneum conductivity, and the peak potential increased with increasing conductivity. Altering the conductivity of the hypodermis, did not result in any differences in the peak potential at any of the nerve fiber locations.

Table 3: The peak potential and activation threshold ratio change for the range of investigated conductivities for the different skin layers in the model. The conductivity values used in the model are reported in parenthesis.

Tissue	Conductivity range (S/m)	Intra-epidermal design			Planar Concentric design		
							
		Max potential change for the A β -fiber	Max potential change for the A δ -fiber	Max change in nerve fiber activation ratio	Max potential change for the A β -fiber	Max potential change for the A δ -fiber	Max change in nerve fiber activation ratio

		loc ati on	loc ati on		loc ati on	loc ati on	
Stratu m Corne um	0.00 002- 0.00 2 [26], [27] (0.0 0004 16)	0. 30 m V	4. 1 m V	0%	0. 31 m V	24 .3 m V	0.03 %
Epider mis; horizo ntal directi on	0.58 - 1.32 [28] (0.9 5)	13 2. 8 m V	1. 5 V	15%	53 .8 m V	22 3. 4 m V	4%
Epider mis; Vertic al directi on	0.13 - 0.17 [28] (0.1 5)	49 .8 m V	25 .8 m V	13%	12 .5 m V	- 97 .6 m V	13%
Dermi s; Horizo ntal directi on	1.74 -3.4 [28] (2.5 7)	86 m V	53 m V	21%	78 .2 m V	- 49 .9 m V	20 %
Dermi s;	1.29 -	37 .4	28 .3	10%	38 .6	34 .8	9%

Vertical direction	1.95 [28] (1.6 2)	m V	m V		m V	m V	
Hypodermis	0.01 -0.1 [27], [29] (0.0 23)	0 V	0 V	0%	0 V	0 V	0%

2.5 Area of selective activation of small fibers

The optimized electrode design parameters were combined for both the planar and intra-epidermal electrodes. The optimized electrodes were subsequently analyzed and compared to the original electrode design of an existing planar concentric electrode introduced by Kaube et al [1], and intra-epidermal electrode introduced by Inui et al [2]. The area of selectivity and the ratio between the activation thresholds for the A β -fiber model and the A δ -fiber model were calculated for both the original and optimized designs. The area of selectivity was defined as the area within which the electrical potential produced by the electrode resulted in a lower activation threshold for the A δ -fiber model than the A β -fiber model. An iterative search was performed to estimate the area of selectivity at different termination depths of the A δ -fiber model. Termination depths of 21 μm , 41 μm , 61 μm , 81 μm , and 101 μm were investigated. The A δ -fiber model was for each iteration moved further away or closer to the center of the electrode based on the activation thresholds of the two nerve fiber models. When the activation threshold of the A δ -fiber model was lower than that of the A β -fiber model, the A δ -fiber model was moved further away from the electrode center. When the threshold of the A δ -fiber model was higher than that of the A β -fiber model, the A δ -fiber model was moved closer to the center of the electrode. The step size with which the A δ -fiber model was moved was halved when the evaluation of the activation thresholds of the previous iteration was opposite to the evaluation of the present iteration. The search was terminated when the difference in activation threshold between the two fiber models were less than 10 μA . The initial step size was 50 μm , and the initial location of the nerve fiber models were directly under the cathode. For the intra-epidermal design the stratum corneum was penetrated by a needle cathode

and, therefore, the initial location of the A δ -fiber model at the 21 μ m depth was shifted by 10 μ m in the horizontal direction away from the cathode edge.

3. Results

3.1 Cathode area

The optimal value of the cathode area was at the lower bound; $2.83\text{e-}3 \text{ mm}^2$ and $6.59\text{e-}4 \text{ mm}^2$ for the planar and intra-epidermal design, respectively. With decreasing cathode area, the potential in the epidermis increased, leading to a decrease in the activation threshold of the A δ -fiber model (see figures 4 and 5). The activation threshold of the A β -fiber likewise decreased, however, the slope was not as steep. Changing the cathode area affected the potential in both the epidermis and dermis, however, the effect on the peak electrical potential in the epidermis was substantially larger than the effect on the peak potential in the dermis. From the largest to the smallest cathode area the peak potential increased by approximately 20 V in the epidermal skin layer compared to approximately 0.4 V in the dermal skin layer.

For the planar design, the optimal cathode area corresponded to a cathode diameter of approximately 60 μ m and gave rise to a threshold activation ratio of 1.77 between the A δ -fiber and the A β -fiber model. In comparison, the ratio for the dimensions of the existing planar concentric electrode [1] was 1.02. For the planar concentric design to be able to activate the small A δ -fiber model at a lower intensity than the large A β -fiber model, the area of the cathode had to be less than 0.085 mm^2 , corresponding to a cathode diameter of approximately 0.33 mm.

For the intra-epidermal design, the optimal cathode area corresponded to an angle of approximately 26 degrees, which gave rise to an activation threshold ratio of 2.4 between the two nerve fiber models. However, the gain in the activation threshold ratio was very limited for cathode areas below 0.01 mm^2 corresponding approximately to an angle of 124 degrees. This is also clear when comparing the optimized activation threshold ratio with the dimensions of the existing intra-epidermal electrode, which had a cathode area of $1.45\text{e-}3 \text{ mm}^2$, and produced an activation threshold ratio between the two nerve fiber models of 2.3. For the intra-epidermal design, the cathode area had to be less than 0.13 mm^2 for the electrode design to preferentially activate the A δ -fiber model, corresponding to a needle angle of approximately 162 degrees.

Electrical potential and cathode area

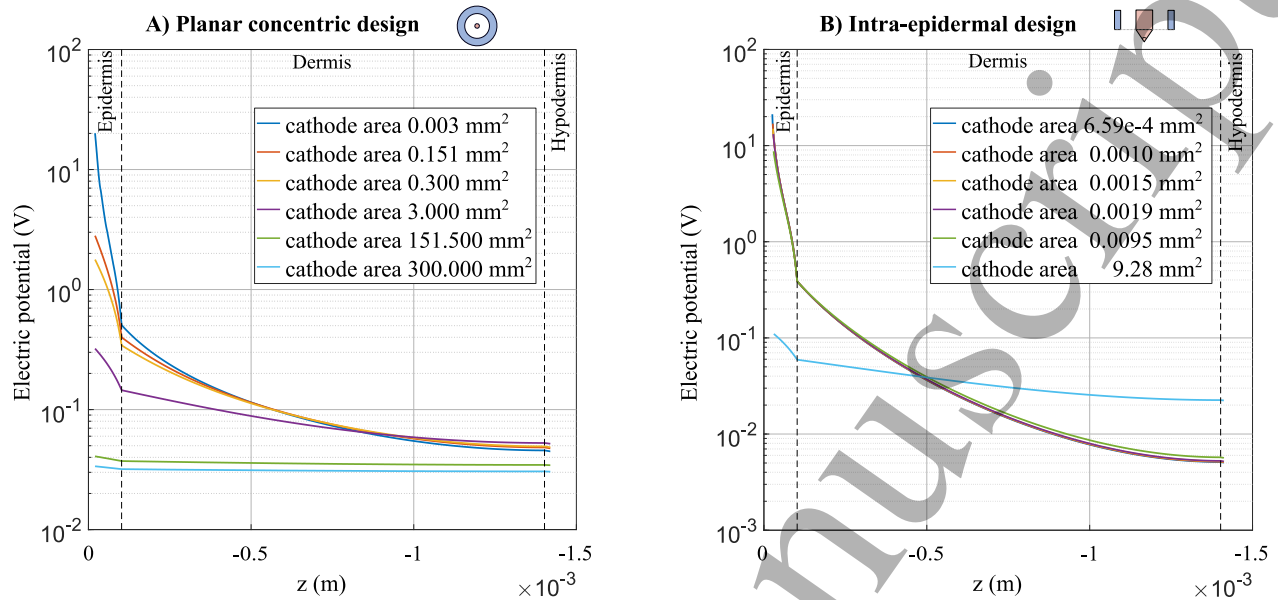


Figure 4: The electrical potential down a straight line directly under the cathode, for the planar concentric (A) and intra-epidermal design (B), at multiple cathode areas.

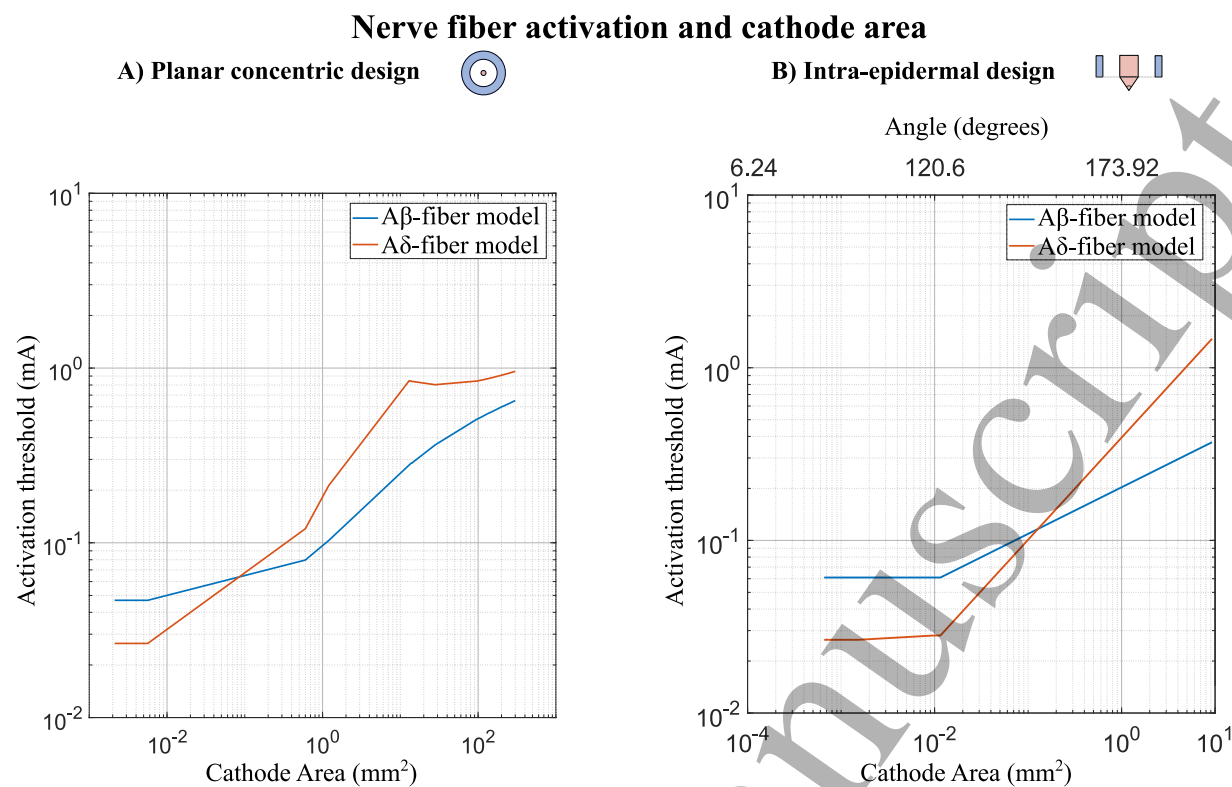


Figure 5: Activation threshold of the two nerve fiber models as a function of cathode area for the planar concentric (A) and intra-epidermal (B) design.

3.2 Cathode Protrusion

The activation threshold ratio was optimized at a cathode protrusion depth of 30 μm (activation threshold ratio was 32.1), 60 μm (activation threshold ratio was 13.6), or 100 μm (activation threshold ratio was 2.2), depending on the nerve fiber location. However, a limited change was seen in the activation threshold ratio, as the A β -fiber model was not affected by cathode protrusion and the A δ -fiber activation was mostly affected for the deep fiber location ($z = -100 \mu\text{m}$) (see figure 6A). Likewise, for the electrical potential in a straight vertical line under the cathode, the relative change in the potential was larger in the deep parts of the dermal skin layer (5-65 %) than in the superficial epidermis (0.1-40%) (see figure 6B).

Intra-epidermal design

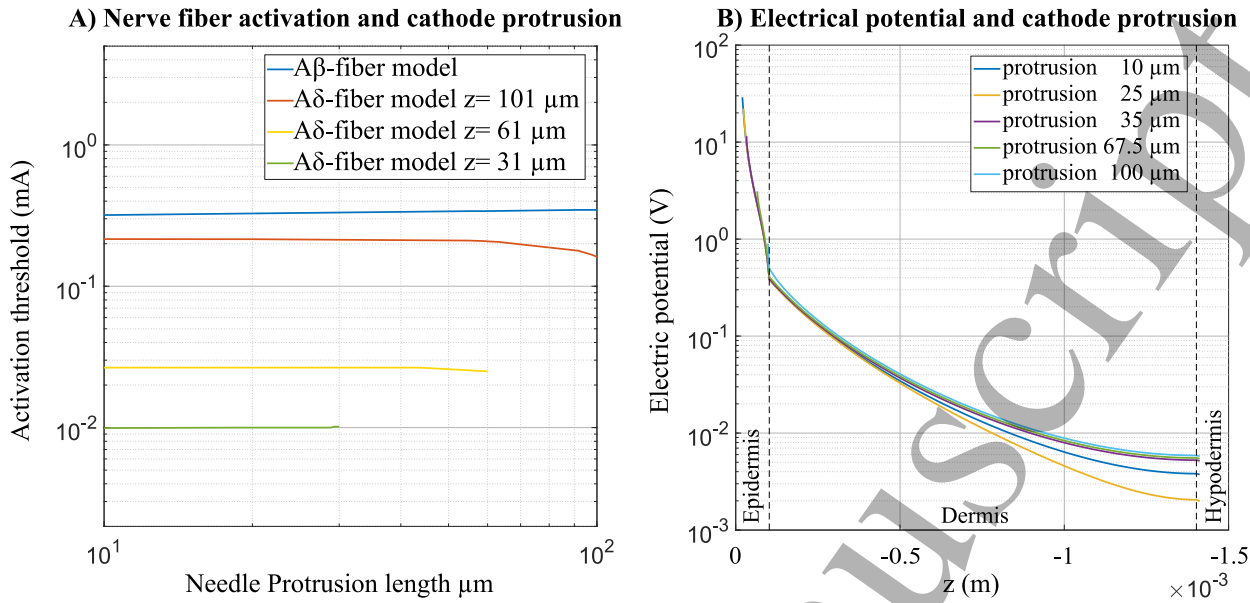


Figure 6: (A) Activation threshold of the two nerve fiber models as a function of cathode protrusion. Three termination depths of the A δ -fiber is presented, and the upper limit for the protrusion was 1 μm above the location of the nerve fiber tip, explaining the difference in protrusion length between nerve fiber locations. (B) The electrical potential down a straight line directly under the cathode, for multiple cathode protrusion depths.

3.3 Anode-cathode distance

The activation threshold ratio between the two nerve fiber models was maximized at an anode-cathode distance of 100 μm . The maximized ratio was 3.08 and 1.22 for the intra-epidermal and planar concentric design, respectively. The electrical potential was mainly affected in the dermal skin layer (see figure 7), where the peak potential dropped by 59% for the intra-epidermal design and 34% for the planar concentric design. The difference in dermal potential from the smallest to the largest anode-cathode distance, continued to increase throughout the dermis. The low potential generated in the dermis resulted in an increase in the activation threshold of the A β -fiber model and consequently an increase in the activation threshold ratio between the two nerve fiber models (see figure 8). For the planar concentric design, the A δ -fiber model was only activated at a lower intensity than the A β -fiber model when the anode-cathode distance was less than 2.9 mm.

Electrical potential and anode-cathode distance

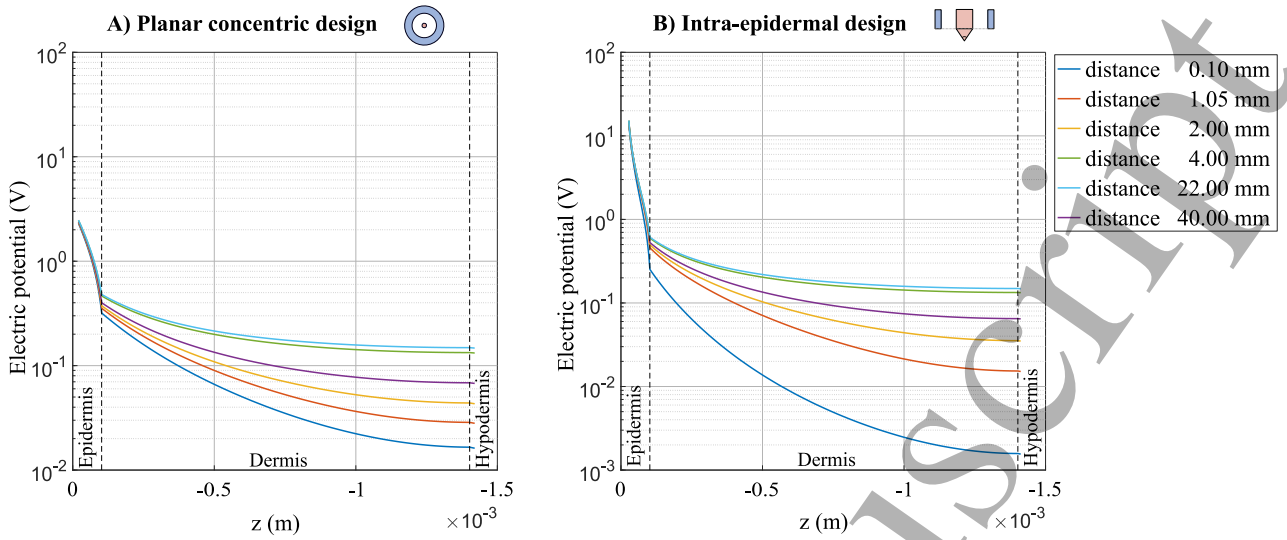


Figure 7: The electrical potential down a straight line directly under the cathode, for the planar concentric (A) and intra-epidermal design (B), at multiple anode-cathode distances.

Nerve fiber activation and anode-cathode distance

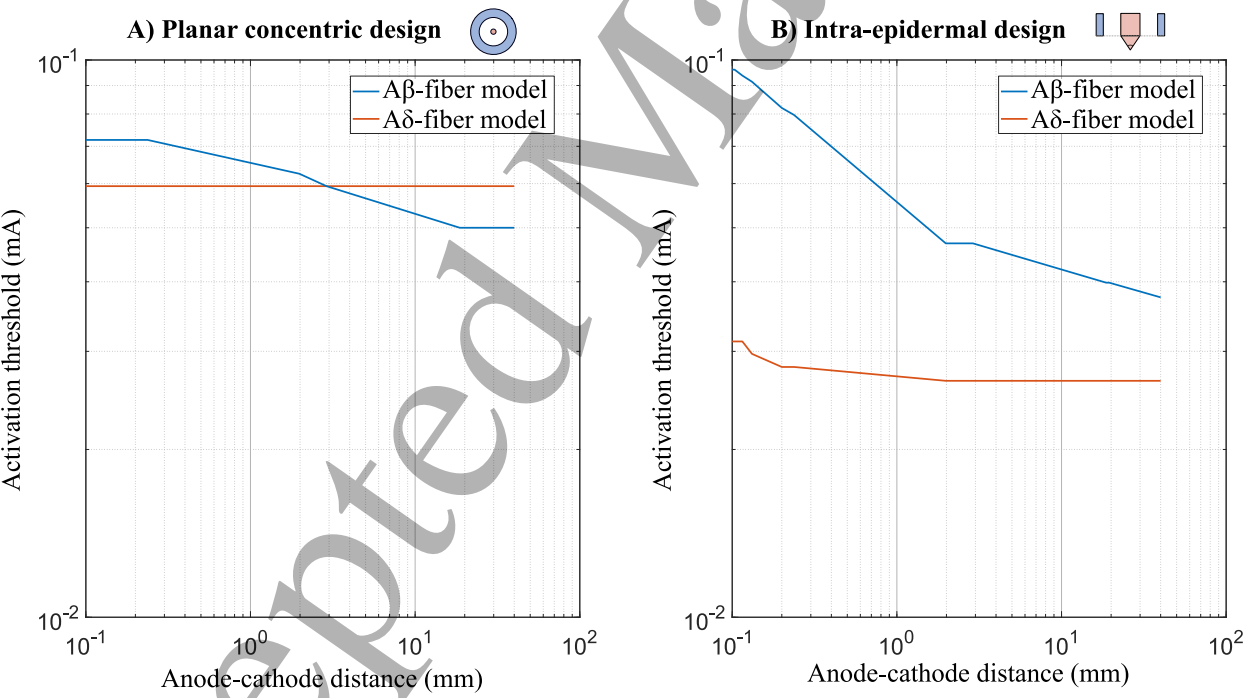


Figure 8: Activation threshold of the two nerve fiber models as a function of anode-cathode distance for the planar concentric (A) and intra-epidermal (B) design.

3.4 Anode area

The maximum activation threshold ratio achieved when optimizing the anode area was 2.3 and 1.03 for the intra-epidermal and planar concentric design, respectively. The maximum ratio was obtained with an anode area of 0.06 mm^2 for both electrode designs. From figure 9 (most pronounced for the intra-epidermal design), it is evident that with a smaller anode area, the current spread to the dermal layer was decreased but the current in the epidermis was relatively unchanged. The decreased electrical potential produced in the dermis caused an increase in the activation threshold of the A β -fiber model and thereby an increase in the activation threshold ratio between the two nerve fiber models (see figure 10). For the planar concentric design, the small A δ -fiber model was only activated at a lower intensity than the large A β -fiber model when the anode area was less than 14 mm^2 . The increase in activation threshold ratio was very limited when the anode area became lower than approximately 9.6 mm^2 and 0.2 mm^2 , for the planar concentric and intra-epidermal design, respectively.

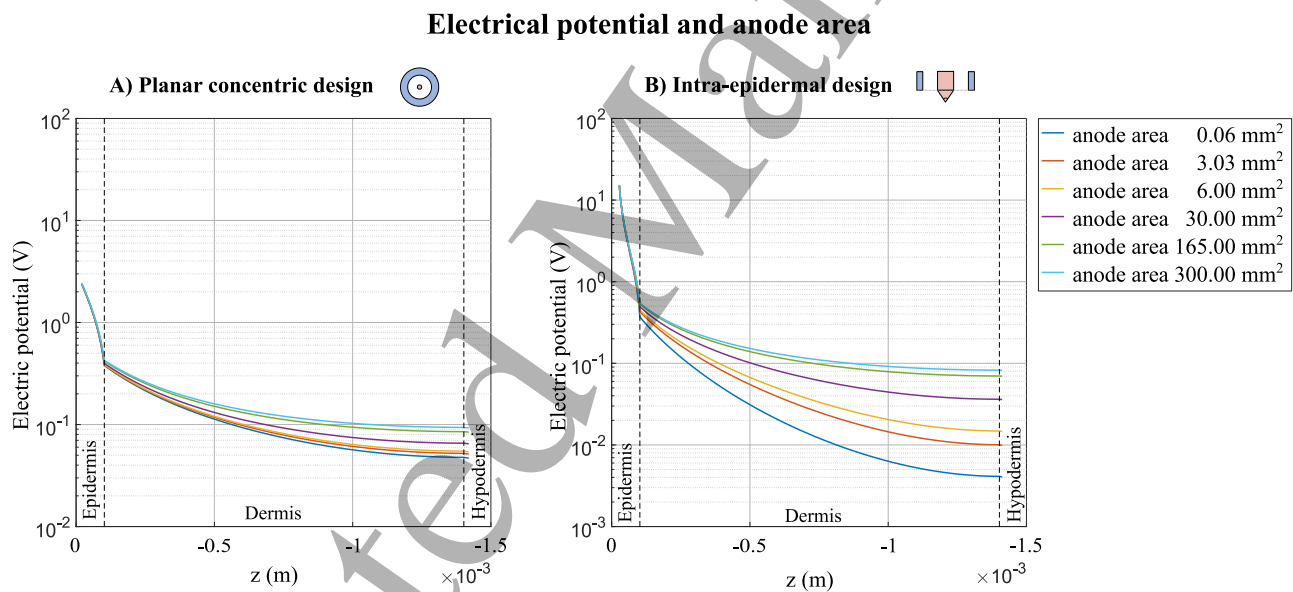


Figure 9: The electrical potential down a straight line directly under the cathode, for different anode areas, for the planar concentric (A) and intra-epidermal design (B).

Nerve fiber activation and anode area

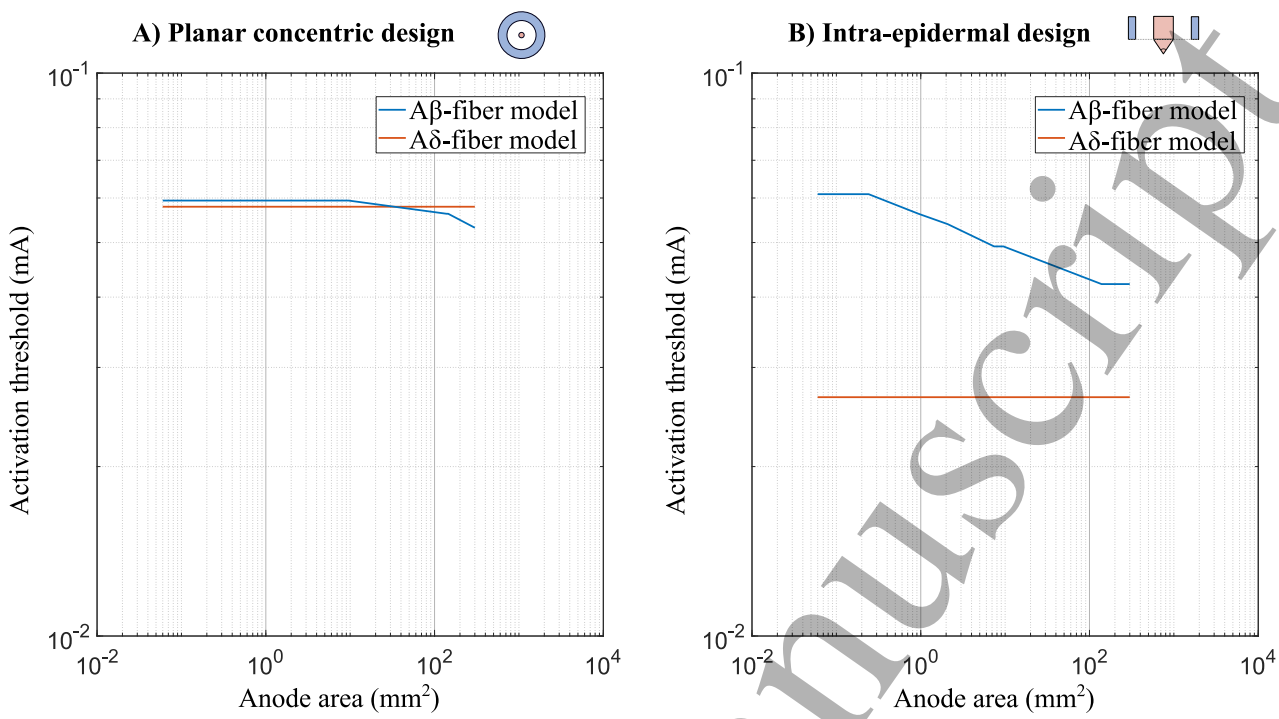


Figure 10: Activation threshold of the two nerve fiber models as a function of anode area for the planar concentric (A) and intra-epidermal (B) design.

3.5 Optimized electrode dimensions

The optimal electrode design parameters were all equal to the respective lower bounds of the optimization algorithm. Indicating that minimizing electrode dimensions improves the electrodes' ability to activate small nociceptive fibers without concomitant activation of large non-nociceptive fibers. The dimensions corresponding to the optimization values of the electrode design parameters and the original dimension of the existing planar concentric [1] and intra-epidermal [2] electrodes are shown in figure 11.

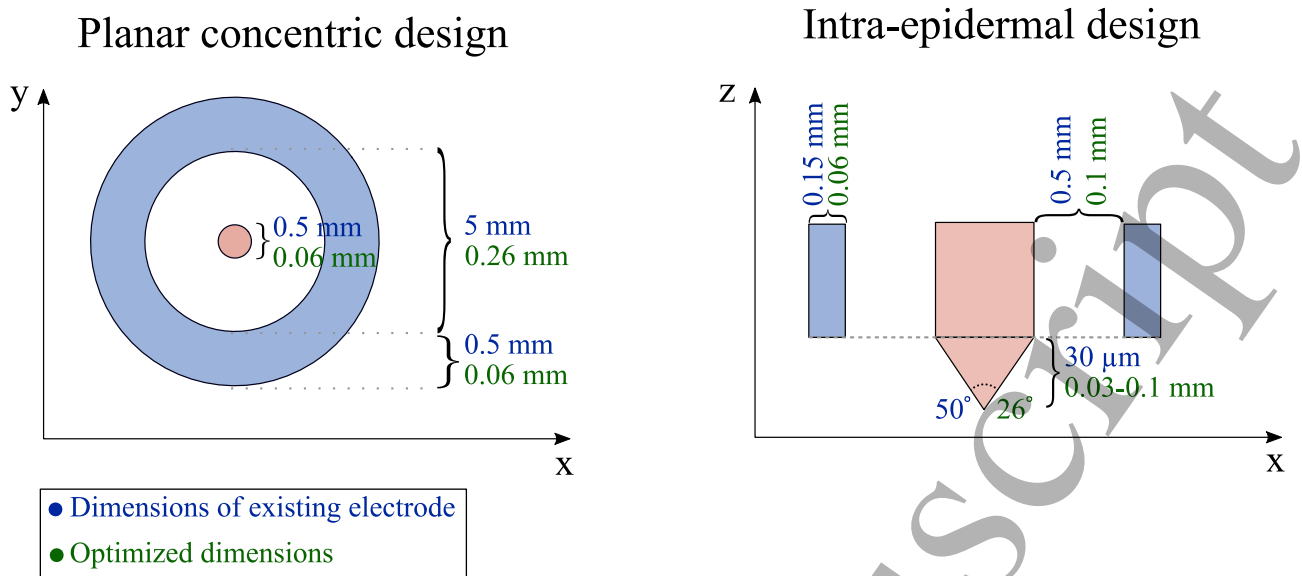


Figure 11: The optimized electrode dimensions and dimensions of the existing planar concentric [1] and intra-epidermal [2] electrodes. The electrode sketches were adapted from the electrode illustrations of [10] .

Comparing the original electrode dimensions to the optimized dimensions for each of the different parameters it was clear that the most gain in preferential small fiber activation was achieved from optimization of cathode area and anode-cathode distance (see figure 12). By optimization of the anode-cathode distance, the percentage increase in nerve fiber activation threshold ratio was 31.32% for the intra-epidermal electrode and 19.61% for the planar concentric electrode. For the cathode area, the activation threshold ratio between the two nerve fiber models increased by 4.84% and 77.79% for the intra-epidermal and planar concentric design, respectively. Optimization of the anode area on its own had the smallest effect with only 0.002 % increase in activation threshold ratio for the intra-epidermal electrode and a 0.83% increase for the planar concentric electrode. Combining the optimized parameters gave rise to a larger increase than for the individual parameters. For the intra-epidermal electrode, the combination of the optimized dimensions increased the activation threshold ratio by 94.69% from the original dimensions. The planar concentric electrode design had the largest potential for improvement, which was seen by the 321.90% increase in the activation threshold ratio for the combination of the optimized parameters compared to the original electrode dimensions.

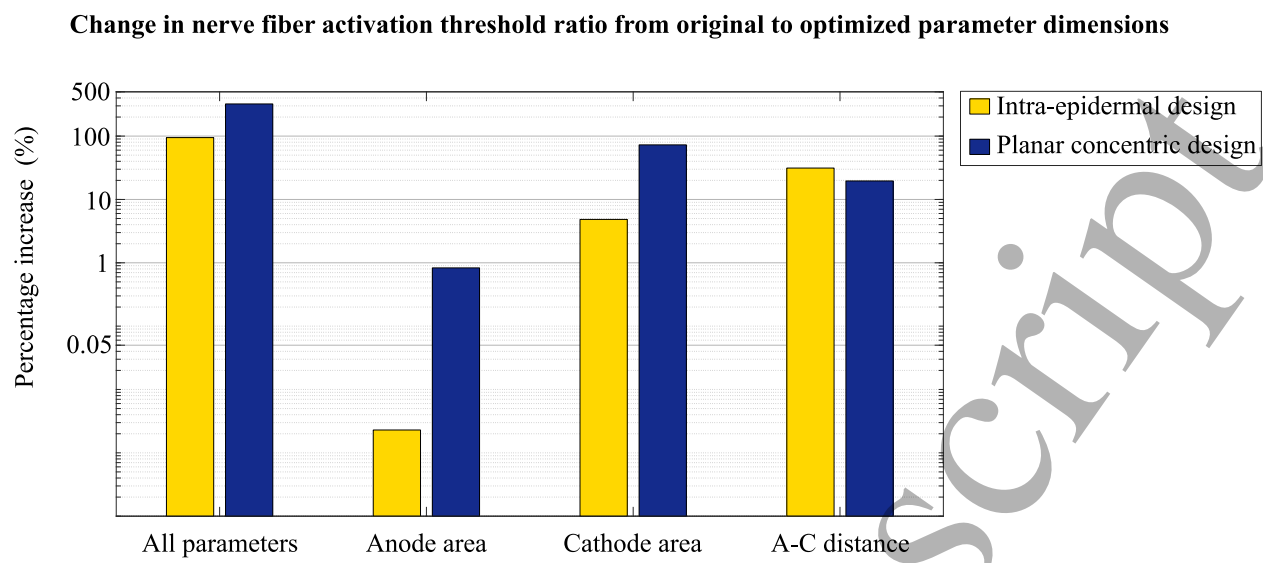


Figure 12: Comparison of the original and optimized electrode design dimensions. The bar plot shows the relative increase in the activation threshold ratio between the two nerve fiber models for each of the optimized parameters.

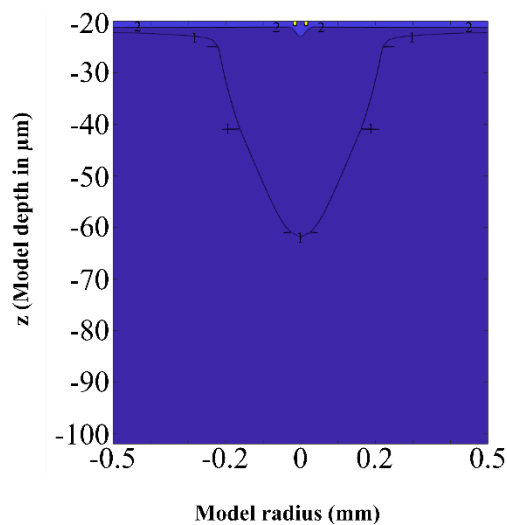
3.6 Area of selectivity

The area of selectivity decreased from the original electrode dimensions to the optimized dimensions (see figure 13). The maximum selective area in the superficial epidermis decreased from 0.20 mm² to 0.01 mm² and from 0.12 mm² to 0.007 mm² for the planar concentric and intra-epidermal design, respectively. However, the maximum activation threshold ratio between the nerve fiber models increased from the dimensions of the existing electrodes to the optimized design dimensions. For the superficial location of the Aβ-fiber model, and the location of the Aδ-fiber model in the middle of the epidermis the activation threshold ratio increased from 2.3 to 4.6 for the intra-epidermal and from 1.02 to 4.3 for the planar concentric design. The increase in the activation threshold ratio for the optimized dimensions was larger when the Aδ-fiber was located closer to the skin surface. At the deepest Aδ-fiber location (z = -101 μm) the activation threshold ratio between the two nerve fiber models was 0.36 for both the optimized intra-epidermal and planar concentric design. This corresponded to an increase from the original dimensions of 25 % for the intra-epidermal design and 92 % for the planar concentric design. The maximum achieved increase in activation threshold ratio was 289 % and 595 % for the intra-epidermal and planar concentric design, respectively. This was observed a few micrometers below the junction of the viable epidermis and the stratum corneum (z = -25 μm) where the activation threshold ratio

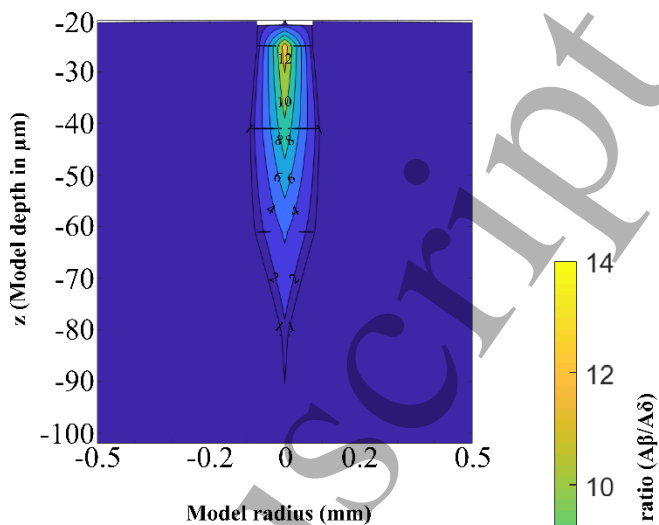
between the two nerve fiber models was 14 for the optimized intra-epidermal design and 13.2 for the optimized planar concentric design.

Additionally, the termination depth of the A δ -fiber model, for which the electrodes could achieve selective stimulation directly under the cathode was increased for the optimized electrode dimensions. This was most pronounced for the planar concentric design as the depth of preferential activation directly under the cathode increased from 61 μm to 84 μm , corresponding to one-half and approximately two-thirds of the epidermal thickness, respectively. For the intra-epidermal design, the increase was from 82 μm to 90 μm in the model, corresponding to a preferential depth down to approximately two-thirds and four-fifths of the epidermis, respectively.

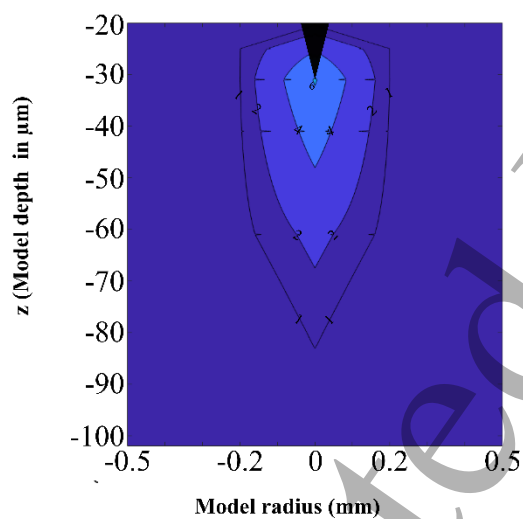
Existing electrode dimensions: Planar concentric electrode



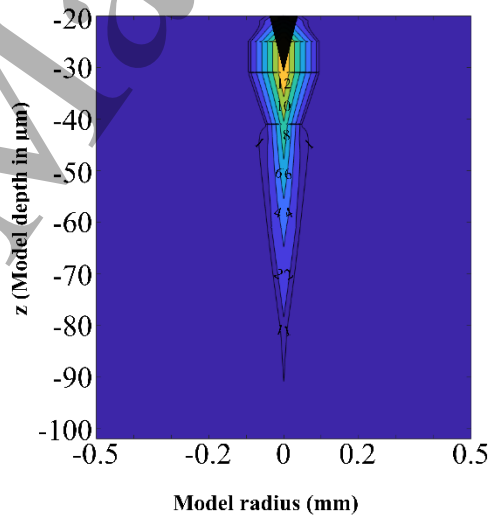
Optimized dimensions: Planar concentric design



Existing electrode dimensions: Intra-epidermal electrode



Optimized dimensions: Intra-epidermal design



Current activation threshold ratio ($A\beta/A\delta$)

Figure 13: Interpolated plot of the radius for which the original and optimized electrode dimensions generated an electrical field that resulted in a lower activation threshold for the $A\delta$ -fiber model than the $A\beta$ -fiber model. The plot shows only the epidermis and was interpolated between calculations of the area of selectivity for $A\delta$ -fiber model depths of $z = -21 \mu\text{m}$, $-41 \mu\text{m}$, $-61 \mu\text{m}$, $-81 \mu\text{m}$, and $-101 \mu\text{m}$, all within the epidermal skin layer. Colors indicate the current activation threshold ratio between the two nerve fiber models and the black area indicates the protruding needle of the intra-epidermal design.

4. Discussion

All the electrode parameters, except the needle protrusion, were optimized at their respective lower bound, which was set according to fabrication possibilities. The needle protrusion was optimal at a few micrometers above the location of the A δ -fiber model. The combined optimized electrode parameters produced a smaller area of selective A δ -fiber activation, but substantially increased the activation threshold ratio between the nerve fiber models and the depth within the epidermis for which preferential activation of small fibers could be achieved.

4.1 Cathode dimensions

Small area electrodes limit the current spread and produce a more superficial current density [7]. The electrodes developed for small fiber activation have taken advantage of this relationship between electrode size and current density distributions and thus all have small cathode areas. These electrodes have been shown to elicit pinprick-like sensations, related to A δ -fiber activation [1]–[4], [30]. This corresponds well with the findings of the present study for which it was likewise observed that smaller cathode areas produced higher electrical potentials in the epidermal skin layers and resulted in lower activation thresholds of the A δ -fiber model. The cathode area of the planar concentric design was estimated only to be small fiber preferential when the cathode area was less than 0.085 mm², corresponding to a cathode diameter of 0.33 mm. This is smaller than the findings of Mørch et al [7], who found that the cathode diameter should be less than 4 mm to achieve preferential activation of small A δ -fibers. The difference could be due to differences in the discretization of the measurement points. The termination depth of the nerve fiber models may also account for some of the differences between the two studies. Mørch et al [7] included a random but uniform distribution of nerve fiber termination depths, however, to reduce the computational load and runtime of the optimization, the termination depth in the present study was fixed. Including more locations of the nerve fibers would likely increase the diameter of the cathode for which preferential small fiber activation can be achieved, due to the continuous drop in the electrical potential throughout the dermal layer. However, the optimized value of the dimension of electrode parameters would not be expected to differ, as the models' termination depths were very conservative.

For the intra-epidermal design, the cathode area had to be less than 0.13 mm^2 for this design to be small fiber preferential, which corresponds to an angle of the cathode needle of 162 degrees. At this point, the electrode is close to planar, and would not likely penetrate the skin. Therefore, an intra-epidermal electrode design is expected to be preferential for small fibers but it requires that it penetrates the stratum corneum. With pointier needles, the electrode may be slightly more preferential for small fibers, however, the smaller the electrode the more local the stimulation area, which may make the electrode less clinically relevant. The optimal protrusion of the cathode did as expected, depend on the termination depth of the target fiber, and was estimated to be optimal a few micrometers above the nerve fiber termination point. This is in line with the findings of Motogi et al [8], who additionally found a shallower protrusion depth to produce a higher in situ electrical field in the superficial skin layers than did a deeper penetrating cathode. They, therefore, suggested that a minor penetration depth would be beneficial when targeting C-fibers in the skin. The value of using protruding cathodes may thus depend on the intentional use of the electrode and the depth of the target nerve fibers, as the benefits of a protruding cathode increases for deeper lying nerve fibers. Additionally, having an electrode that penetrates the most resistive layer of the skin, the stratum corneum, may improve the impedance.

4.2 Anode dimensions

The dimensions of the anode had very little to no effect on the activation threshold of the $A\delta$ -fiber model (maximum $4 \mu\text{A}$ change), however, it was of high importance for the activation threshold of the $A\beta$ -fiber model. Especially the anode-cathode distance is of high impact. A short distance between the anode and cathode resulted in a limited amount of current reaching the $A\beta$ -fiber model in the dermal skin layer, making it more difficult to activate and thereby increasing the activation threshold ratio between the nerve fiber models. This is in line with the general understanding of current spread in the skin. Motogi et al [8], likewise investigated the anode-cathode distance for the intra-epidermal electrode, but opposite to the findings of the present study, they found little effect on the peak electrical field through the skin layers. They only investigated three distances, and no distances less than 1.3 mm, which may explain why they did not find any differences in the electrical field in the dermal layer. From figure 7 and 8, it is clear that the electrical potential within the dermis is greatly decreased for short anode-cathode distances and that the slope of the

activation threshold of the A β -fiber model becomes very steep when the anode-cathode distance decreases to less than 1.5 mm, and thereby increase the preferential activation of the A δ -fiber model. The same tendency was observed for the planar concentric electrode, for which the anode-cathode distance needed to be less than 2.9 mm for the electrode to be preferential for the A δ -fiber model.

The size of the anode likewise contributed to an increased activation threshold of the A β -fiber model, however, to a much lesser degree than the anode-cathode distance. Verhoeven and Van Dijk, 2006 [31], investigated the H-reflex in relation to the anode size and the pain experienced during stimulations. They found that with a small anode area (36 mm²) subjects tended to describe the sensation of the stimulation as sharp and cutting, whereas they for the large anode area (1,296 mm²) chose words like pressing and gnawing to describe the sensation [31]. Furthermore, participants rated the pain higher for the small anode area, suggesting that the small anode area activated more cutaneous nociceptors [31]. This may be explained by the findings of the present study as a smaller anode area reduced the current spread to deeper tissues, thereby increasing the electrical potential difference between the superficial and deeper skin structures, leading to more preferential activation of pain mediating A δ -fibers.

4.3 Optimized electrode dimensions

Combining the individually optimized electrode design parameters in an optimized electrode design increased the activation threshold ratio between the A β -fiber model and the A δ -fiber model by 94.69 % and 321.90 % for the intra-epidermal and planar concentric design, respectively. The difference in activation threshold ratio was mainly due to a large increase in the activation threshold of the A β -fiber model, indicating the large influence of the anode on the depth of the current spread and thereby nerve fiber activation. It is thus clear that it is important to optimize both the cathode as well as the anode in order to improve preferential small fiber activation. For the existing intra-epidermal electrode, Mouraux et al [11] concluded that stimulation intensities should be below two times the perception threshold to ensure preferential activation of small fibers. The model predicted a maximum activation threshold ratio between the two nerve fiber models of 1.9 and 3.6 for the existing planar concentric and intra-epidermal electrode dimensions,

respectively. Considering the model estimates of the activation threshold as a rough approximation of perception thresholds, calculated from an average representation of the nerve fiber population [10], [20] the model predictions correspond well with the findings of Mouraux et al [11]. For the optimized electrode design parameters, the model predicted a maximum activation threshold ratio of 14 and 13.2 for the intra-epidermal and planar concentric design, respectively. Indicating, that by electrode optimization it might be possible to increase the feasible intensity range of preferential small fiber activation to around 10 times perception threshold.

The small area of the optimized electrode design, however, may impose other issues, as the impedance increases with a smaller electrode area. Higher impedances increase the requirements for stimulator compliance. This could potentially mean that clinically available stimulators would not be able to deliver the necessary voltages or that only low intensities can be applied. Additionally, as the electrode area decreases the area of selectivity decreases. Having small electrodes makes the stimulation area more localized and is thereby able to activate fewer nerve fibers. This very localized stimulation makes the use of the electrode, less clinically feasible as the electrode needs to be located very close to the nerve fiber and may have to be moved multiple times to achieve perception [9], [32]. To overcome this issue Inui and Kakigi et al [32] suggested the use of multiple electrodes or electrodes with multiple cathodes. Poulsen et al [10] compared the planar concentric electrode and the intra-epidermal electrode with a pin and planar array electrode, with 15 and 12 small cathodes, respectively. It was found that the use of multiple cathodes obtained a similar preferential activation as the other single cathode electrodes, but increased the area of selectivity, which would be beneficial in a clinical setting. Additionally, adding multiple cathodes or electrode pairs would increase the total electrode area and thereby decrease the impedance and the demands on stimulator compliance. This is, however, provided that all interfaces between the cathodes and the skin has equal impedance, which would not be the case if one of the cathodes have a poor skin contact or is located in close proximity to a low-impedance skin appendage.

4.4 Preferential activation of small fibers and nerve fiber location

The original dimensions of the planar concentric electrode activated the A δ -fiber model at approximately the same intensity as the A β -fiber model (activation threshold ratio 1.02). Poulsen et al [10] displayed an activation threshold ratio between the two nerve fiber models of 1.5 and 5.9

with a rectangular stimulation pulse of 0.1 and 10 ms, respectively. This is a higher ratio than in the present study, which is due to the location of the A β -fiber model. Poulsen et al [10] had the A β -fiber model located in the middle of the dermis instead of the superficial location in the present study. For the optimization and simulations in the present study, the A β -fiber model was located in the superficial dermis, to investigate if selective activation of small epidermal nerve fibers could be achieved. However, in hairy skin, the myelinated nerve fibers are most abundant around hair follicles and only a few fibers terminate in the superficial dermis [6]. Since single fiber activation is not enough to produce perception [33] and the electrode area of the planar concentric electrode is small it could be argued that superficial A β -fibers are not activated to a detectable degree. This may be the reason why pinprick like sensations and late EEG responses have been observed [12], [13] even for the original dimensions of the planar concentric electrode. However, the performance of the electrode is still highly debated as La Cesa et al [18] found the pricking sensation to be abolished after application of topical capsaicin, but no changes were evident in the EEG response, indicating that concomitant activation of large A β -fibers does occur even at low stimulation intensities. Suggesting, that activation of the superficially located A β -fibers does occur.

For the optimized electrode dimensions, the model predicted that coactivation of A β -fibers will no longer occur as the planar concentric electrode design became selective for small fibers down to approximately two-thirds of the epidermal thickness. This increase in the depth for which small fibers may be activated at a lower intensity than large fibers is especially important if the electrode is to be used to assess small fiber neuropathy. In small fiber neuropathy loss and retraction of intra-epidermal nerve fibers have been observed [19], [34]. The retraction of the nerve fibers means that their termination depth becomes greater and they thereby lie further from the skin surface. With existing electrodes, it would thus be difficult to activate the small fibers without co-activating a large number of large fibers, and thereby lose the information of small fiber function and integrity, when the small fibers start to retract due to small fiber neuropathy. However, with the optimized electrode design parameters, the model predicted that it will be possible to achieve preferential small fiber activation deep in the epidermal layer and thereby enable the possibility to assess small fiber function in patients with small fiber neuropathy and perhaps even diagnose and follow the progression of the disease.

4.5 Study limitations

Several simplifications of the model were implemented to reduce computational complexity. To reduce complexity and computational time the electrode materials were not modelled, instead a normal current density was applied to the contact surface of the skin to simulate the electrode. Adding the electrode material would have enabled the modelling of the differences in current density that may arise across the electrode, however, due to the small size of the simulated electrodes, these differences were expected to be small and should not affect the results of the nerve fiber models. The junctions between skin layers were modeled as horizontal planes and skin appendages were omitted from the model. However, appendage structures such as sweat ducts have a large influence on the current spread as they establish a low resistance pathway for the current to reach deeper tissues [35]. Consequently, if the electrode is positioned upon a sweat duct the possibility of activating the deeper lying A β -fibers increases. However, as the dimensions in the optimized electrodes are small, the likelihood of placing the electrode at an appendage is minimal. Blood vessels may also affect the current spread in their close proximity via a shunting effect [36]. However, including the vessels in the present model is not expected to have an effect due to the location of the nerve fibers and the size of blood vessels within these areas. The A δ -fiber model was activated at the tip, which is located in the avascular epidermis. The A β -fiber model was likewise activated at the tip, which was located in the superficial dermis, where only small capillaries are located and therefore not expected to have significant effects on the potential.

Hydrated skin has a higher conductivity than dry skin and hence the moisture content of the skin will affect the current spread. This was also evident in the sensitivity analysis of the tissue conductivities, which revealed the potential to change by up to approximately 1.5 V when increasing the conductivity of the different skin layers. The moisture content of the stratum corneum has a high impact on impedance values and may change over the time course of stimulation as the transepidermal water loss increases when applying electrical stimulation [37]. Apart from hydrating the stratum corneum, the increase in transepidermal water loss may introduce more moisture to the electrode-skin interface. This increased moisture content in the electrode-skin interface may, due to the small electrode size of the optimized design, pose a risk of shortcircuiting the cathode and anode. This has, however, not been reported as an issue for other electrodes of similar sizes [4], and is therefore not expected for the proposed design dimensions in the present study. Furthermore, the steady-state solution was used for calculating the electrical potentials in the skin, disregarding the capacitive properties [10], [20] (supplementary materials).

The nerve fiber models were simplified to single fibers representing the average of the respective nerve fiber populations. The spatial distribution of nerve fibers in the skin was only partly considered for the A δ -fiber nerve in the calculation of the area of selectivity, where locations for which an A δ -fiber could be activated selectively was estimated. Previous validation of the model have shown that even with the specified simplifications, the model is able to predict experimental perception thresholds [10], [20]. It is likely that the average representation of the nerve fiber population is able to predict perception thresholds because the action potential is generated either at the tip or at the first node of ranvier.

5. Conclusion

There are two important aspects to consider when designing electrodes for small fiber activation. First of all to enable preferential activation of small fibers a high current density in the superficial skin layer, where these fibers terminate, is crucial. This can be achieved by small area cathodes. Secondly, the current spread to deeper tissue layers need to be limited to prevent large fiber activation. To this end, the anode dimensions are important as a small anode area and a small distance between the anode and cathode will cause the current to be concentrated superficially.

The area of selectivity was decreased for the optimized electrode designs. However, the epidermal depth for which they could achieve preferential activation was increased and the optimized design increased the preferential activation of small fibers substantially, by increasing the activation threshold ratio between the two nerve fiber models by 92-595 % for the planar concentric electrode design and 25-289 % for intra-epidermal electrode design, depending on the termination depth of the activated A δ -fiber.

Acknowledgments

1
2
3
4
5
6
7
8
9
10
11
12
13
14
15
16
17
18
19
20
21
22
23
24
25
26
27
28
29
30
31
32
33
34
35
36
37
38
39
40
41
42
43
44
45
46
47
48
49
50
51
52
53
54
55
56
57
58
59
60

The authors have no conflict of interest to declare. The presented work has been funded by the Center for Neuroplasticity and Pain (CNAP), supported by the Danish National Research Foundation (DNRF121).

Accepted Manuscript

References

- [1] Kaube, H., Katsarava, Z., Käufer, T., Diener, H.-C., and Ellrich, J., 2000, A new method to increase nociception specificity of the human blink reflex, *Clin. Neurophysiol.*, **111**, 413–416.
- [2] Inui, K., Tran, T. D., Hoshiyama, M., and Kakigi, R., 2002, Preferential stimulation of A δ fibers by intra-epidermal needle electrode in humans, *Pain*, **96**, 247–252.
- [3] Lelic, D., Mørch, C. D., Hennings, K., Andersen, O. K., and Drewes, A. M., 2012, Differences in perception and brain activation following stimulation by large versus small area cutaneous surface electrodes, *Eur. J. Pain*, **16**, 827–837.
- [4] Leandri, M., Marinelli, L., Siri, A., and Pellegrino, L., 2018, Micropatterned surface electrode for massive selective stimulation of intraepidermal nociceptive fibres, *J. Neurosci. Methods*, **293**, 17–26.
- [5] Ebenezer, G. J., Hauer, P., Gibbons, C., McArthur, J. C., and Polydefkis, M., 2007, Assessment of epidermal nerve fibers: a new diagnostic and predictive tool for peripheral neuropathies., *J. Neuropathol. Exp. Neurol.*, **66**, 1059–1073.
- [6] Provitera, V., Nolano, M., Pagano, A., Caporaso, G., Stancanelli, A., and Santoro, L., 2007, Myelinated nerve endings in human skin, *Muscle Nerve*, **35**, 767–775.
- [7] Mørch, C. D., Hennings, K., and Andersen, O. K., 2011, Estimating nerve excitation thresholds to cutaneous electrical stimulation by finite element modeling combined with a stochastic branching nerve fiber model, *Med. Biol. Eng. Comput.*, **49**, 385–395.
- [8] Motogi, J., Sugiyama, Y., Laakso, I., Hirata, A., Inui, K., Tamura, M., and Muragaki, Y., 2016, Why intra-epidermal electrical stimulation achieves stimulation of small fibres selectively: a simulation study, *Phys. Med. Biol.*, **61**, 4479–4490.
- [9] Mouraux, A., Marot, E., and Legrain, V., 2014, Short trains of intra-epidermal electrical stimulation to elicit reliable behavioral and electrophysiological responses to the selective activation of nociceptors in humans, *Neurosci. Lett.*, **561**, 69–73.
- [10] Poulsen, A. H., Tigerholm, J., Meijs, S., Andersen, O. K., and Mørch, C. D., 2020, Comparison of existing electrode designs for preferential activation of cutaneous nociceptors, *J. Neural Eng.*
- [11] Mouraux, A., Iannetti, G. D., and Plaghki, L., 2010, Low intensity intra-epidermal electrical stimulation can activate A δ -nociceptors selectively, *Pain*, **150**, 199–207.

- [12] Katsarava, Z., Ayzenberg, I., Sack, F., Limmroth, V., Diener, H. C., and Kaube, H., 2006, A novel method of eliciting pain-related potentials by transcutaneous electrical stimulation, *Headache*, **46**, 1511–1517.
- [13] Lefaucheur, J. P., Ahdab, R., Ayache, S. S., Lefaucheur-Ménard, I., Rouie, D., Tebbal, D., Neves, D. O., and Ciampi de Andrade, D., 2012, Pain-related evoked potentials: A comparative study between electrical stimulation using a concentric planar electrode and laser stimulation using a CO₂ laser, *Neurophysiol. Clin.*, **42**, 199–206.
- [14] Suzuki, C., Kon, T., Funamizu, Y., Ueno, T., Haga, R., Nishijima, H., Arai, A., Tomiyama, M., and Baba, M., 2016, Elevated pain threshold in patients with asymptomatic diabetic neuropathy: an intraepidermal electrical stimulation study, *Muscle and Nerve*, **54**, 146–149.
- [15] Mueller, D., Obermann, M., Koeppen, S., Kavuk, I., Yoon, M.-S., Sack, F., Diener, H.-C., Kaube, H., and Katsarava, Z., 2010, Electrically evoked nociceptive potentials for early detection of diabetic small-fiber neuropathy, *Eur. J. Neurol.*, **17**, 834–841.
- [16] Katsarava, Z., Yaldizli, Ö., Voulkoudis, C., Diener, H.-C., Kaube, H., and Maschke, M., 2006, Pain related potentials by electrical stimulation of skin for detection of small-fiber neuropathy in HIV, *J. Neurol.*, **253**, 1581–1584.
- [17] Perchet, C., Frot, M., Charmarty, A., Flores, C., Mazza, S., Magnin, M., and Garcia-Larrea, L., 2012, Do we activate specifically somatosensory thin fibres with the concentric planar electrode? A scalp and intracranial EEG study, *Pain*, **153**, 1244–1252.
- [18] La Cesa, S. *et al.*, 2018, Skin denervation does not alter cortical potentials to surface concentric electrode stimulation: A comparison with laser evoked potentials and contact heat evoked potentials, *Eur. J. Pain*, **22**, 161–169.
- [19] Pittenger, G. L., Ray, M., Burcus, N. I., McNulty, P., Basta, B., and Vinik, A. I., 2004, Intraepidermal Nerve Fibers Are Indicators of Small-Fiber Neuropathy in Both Diabetic and Nondiabetic Patients, *Diabetes Care*, **27**, 1974–1979.
- [20] Tigerholm, J., Poulsen, A. H., Andersen, O. K., and Mørch, C. D., 2019, From Perception Threshold to Ion Channels—A Computational Study, *Biophys. J.*, **117**.
- [21] Chi, Y. M., Jung, T. P., and Cauwenberghs, G., 2010, Dry-contact and noncontact biopotential electrodes: Methodological review, *IEEE Rev. Biomed. Eng.*, **3**, 106–119.
- [22] Hines, M. L. and Carnevale, N. T., 1997, The NEURON Simulation Environment, *Neural Comput.*, **9**, 1179–1209.
- [23] McArthur, J. C., Stocks, E. A., Hauer, P., Cornblath, D. R., and Griffin, J. W., 1998, Epidermal Nerve Fiber

Density, *Arch. Neurol.*, **55**, 1513.

- [24] Luersen, M. A., Le Riche, R., and Guyon, F., 2004, A constrained, globalized, and bounded Nelder-Mead method for engineering optimization, *Struct. Multidiscip. Optim.*, **27**, 43–54.
- [25] Nelder, J. A. and Mead, R., 1965, A Simplex Method for Function Minimization, *Comput. J.*, **7**, 308–313.
- [26] Yamamoto, T. and Yamamoto, Y., 1976, Electrical properties of the epidermal stratum corneum, *Med. Biol. Eng.*, **14**, 151–158.
- [27] Santis, V. De, Chen, X. L., Laakso, I., and Hirata, A., 2015, An equivalent skin conductivity model for low-frequency magnetic field dosimetry, *Biomed. Phys. Eng. Express*, **1**, 1–10.
- [28] Tavernier, A., Dierickx, M., and Hinsenkamp, M., 1993, Tensors of dielectric permittivity and conductivity of in vitro human derms and epiderms., *Bioelectroch. Bioener.*, **30**, 65–72.
- [29] Hasgall, P., F. D. G., C. B., E. N., B. L., MC, G., A. K., and N. K., IT'IS Database for thermal and electromagnetic parameters of biological tissues, *Version 4.0, may 15*, 2018. [Online]. Available: itis.swiss/database.
- [30] Hugosdottir, R., Mørch, C. D., Jørgensen, C. K., Nielsen, C. W., Olsen, M. V., Pedersen, M. J., and Tigerholm, J., 2019, Altered excitability of small cutaneous nerve fibers during cooling assessed with the perception threshold tracking technique, *BMC Neurosci.*, **20**, 1–13.
- [31] Verhoeven, K. and van Dijk, J. G., 2006, Decreasing pain in electrical nerve stimulation, *Clin. Neurophysiol.*, **117**, 972–978.
- [32] Inui, K. and Kakigi, R., 2012, Pain perception in humans: use of intraepidermal electrical stimulation, *J. Neurol. Neurosurg. Psychiatry*, **83**, 551–556.
- [33] Johansson, R. S. and Vallbo, A. B., 1979, Detection of tactile stimuli. Thresholds of afferent units related to psychophysical thresholds in the human hand., *J. Physiol.*, **297**, 405–422.
- [34] Karlsson, P., Hincker, A. M., Jensen, T. S., Freeman, R., and Haroutounian, S., 2019, Structural, functional, and symptom relations in painful distal symmetric polyneuropathies: a systematic review, *Pain*, **160**, 286–297.
- [35] Sha, N., Kenney, L. P. J., Heller, B. W., Barker, A. T., Howard, D., and Moatamedi, M., 2008, A Finite Element Model to Identify Electrode Influence on Current Distribution in the Skin, *Artif. Organs*, **32**, 639–643.
- [36] Lowery, M. M., Stoykov, N. S., Dewald, J. P. A., and Kuiken, T. A., 2004, Volume conduction in an anatomically based surface EMG model, *IEEE Trans. Biomed. Eng.*, **51**, 2138–2147.

- [37] Almalty, A. M. R., Hamed, S. H., Al-Dabbak, F. M., and Shallan, A. E., 2013, Short-term and long-term effects of electrical stimulation on skin properties, *Physiother. Res. Int.*, **18**, 157–166.
- [32] Böhling, A., Bielfeldt, S., Himmelmann, A., Keskin, M., and Wilhelm, K. P., 2014, Comparison of the stratum corneum thickness measured in vivo with confocal Raman spectroscopy and confocal reflectance microscopy, *Ski. Res. Technol.*, **20**, 50–57.
- [33] Rajadhyaksha, M., González, S., Zavislan, J. M., Anderson, R. R., and Webb, R. H., 1999, In vivo confocal scanning laser microscopy of human skin II: Advances in instrumentation and comparison with histology, *J. Invest. Dermatol.*, **113**, 293–303.
- [34] Huzaira, M., Rius, F., Rajadhyaksha, M., Anderson, R. R., and González, S., 2001, Topographic variations in normal skin, as viewed by in vivo reflectance confocal microscopy, *J. Invest. Dermatol.*, **116**, 846–852.
- [35] Sandby-Møller, J., Poulsen, T., and Wulf, H. C., 2003, Epidermal Thickness at Different Body Sites: Relationship to Age, Gender, Pigmentation, Blood Content, Skin Type and Smoking Habits, *Acta Derm. Venereol.*, **83**, 410–413.
- [36] Neerken, S., Lucassen, G. W., Bisschop, M. a., Lenderink, E., and Nuijs, T. (a. M. ., 2004, Characterization of age-related effects in human skin: A comparative study that applies confocal laser scanning microscopy and optical coherence tomography, *J. Biomed. Opt.*, **9**, 274.
- [37] Egawa, M., Hirao, T., and Takahashi, M., 2007, In vivo estimation of stratum corneum thickness from water concentration profiles obtained with raman spectroscopy, *Acta Derm. Venereol.*, **87**, 4–8.
- [38] Yamamoto, T. and Yamamoto, Y., 1976, Electrical properties of the epidermal stratum corneum, *Med. Biol. Eng.*, **14**, 151–158.
- [39] Tavernier, A., Dierickx, M., and Hinsenkamp, M., 1993, Tensors of dielectric permittivity and conductivity of in vitro human derms and epiderms., *Bioelectroch. Bioener.*, **30**, 65–72.
- [40] Krackowizer, P. and Brenner, E., 2008, Dicke der Epidermis und Dermis* sonographische Messung an 24 Stellen des Menschlichen Körpers, *Phlebologie*, **37**, 83–92.
- [41] Gabriel, C., Gabriel, S., and Corthout, E., 1996, The dielectric properties of biological tissues: I. Literature survey, *Phys. Med. Biol.*, **41**, 2231–2249.
- [42] Gabriel, S., Gabriel, C., and W, L. R., 1996, The dielectric properties of biological tissues: II. Measurements in the frequency range 10 Hz to 20 GHz, *Phys. Med. Biol.*, **41**, 2251–2260.